microfabrication applications, it is widely used to transfer the designed patterns from an etching mask to the substrate. When the sample is immersed into the etching bath, the etchant only contacts and reacts with the substrate surfaces where are uncovered by the etching mask. The suitable materials for the mask can be polymers or other materials such as photoresist, SU-8,SiO_2 andSi_3N_4, which feature much lower etching rate in the selected etchant in contrast to the substrate material.

Wet etchants fall into two broad categories: isotropic etchants and anisotropic etchants. Isotropic etchants attack the material being etched at the same rate in all directions. Anisotropic etchants attack some single-crystal materials (typically silicon) at different etch rates depending on the crystallographic orientation of the substrate, so there is more control of the shapes being produced.

Wet etching is the most common processing in semiconductor industry and MEMS applications.

Cross References

- ► Fabrication of 3-D Microfluidic Structures
- ► Microfabrication Techniques
- ► Photolithography
- ► Photoresist Reflow
- ► Wet Chemical Etch

Wettability Patterning

- ► Hydrophilic/Hydrophobic Patterning

Wetting Phenomenon

- ► Surface Tension Driven Flow

Wetting and Spreading

LESLIE YEO
Micro/Nanophysics Research Laboratory
Department of Mechanical Engineering, Monash University, Clayton, VIC, Australia
leslie.yeo@eng.monash.edu.au

Synonyms

Capillarity

Definition

The wettability of a liquid governs how it spreads over a solid substrate or an immiscible liquid phase and is characterized by a contact angle, which is the angle subtended by the liquid/vapor interface and the solid or immiscible liquid surface. Depending on the surface energy of the substrate, two equilibrium situations can occur upon contact of the liquid and the solid. *Complete wetting* corresponds to the situation when the surface energy of the substrate is high and hence the liquid spreads entirely over (or wets) the solid, thereby forming a film in which case the contact angle is zero. *Partial wetting*, on the other hand, relates to the situation when the surface energy of the substrate is low and hence a finite contact angle is obtained in which case the liquid retains its drop shape which is restricted at the solid surface by a contact line where the solid, liquid and vapor phases meet. The governing principle is the minimization of interfacial energy; in the former case, the interfacial contact between the liquid film and the solid substrate minimizes the free energy of the surface.

Overview

Wetting and spreading, the subject of which is a fundamental pillar of colloid and interface science, are fundamental processes which occur in a wide variety of natural and industrial settings. These processes govern the adhesion between two substances and therefore have significant implications in paint, lubrication, coating, printing and fabric technology as well as in enhanced oil recovery. More recently, there has been renewed interest in the relevance of wetting and spreading in biological and microscale environments. The functional design of biomaterials and biological surfaces requires a thorough understanding of the interrelationships of bio-surfaces and bio-environments. The miniaturization of fluid processes, on the other hand, is associated with an increase in the dominance of surface forces over body forces given that the surface area to volume ratio scales as the inverse of the characteristic system dimension. Thus, at microscale dimensions, surface tension and hence wettability (or capillarity) effects are extremely important considerations in the design of microfluidic devices.

Basic Methodology

Surface Tension and Contact Angle

The relationship between surface tension γ and contact angle θ, formally defined as

$$\theta = \cos^{-1}\left(\boldsymbol{n}_{\mathrm{l}}\boldsymbol{n}_{\mathrm{s}}\right), \tag{1}$$

where $\boldsymbol{n}_{\mathrm{l}}$ and $\boldsymbol{n}_{\mathrm{s}}$ are the outward pointing unit normal vectors from the liquid and solid at the three-phase contact line, respectively, was first established by Thomas Young

in 1805 through a force balance in the plane of the surface at the contact line (Fig. 1):

$$\gamma_{LV}\cos\theta = \gamma_{SV} - \gamma_{SL}\,, \tag{2}$$

where the subscripts LV, SV and SL denote the liquid-vapor, solid-vapor and solid-liquid phases, respectively. Equation (2) is thus known as *Young's equation.* It should be noted that a force balance also exists in the plane normal to the surface due to the existence of a strain field beneath the contact line to balance the force component $\gamma_{LV}\sin\theta$. In the case of a liquid lens sitting at the interface of an immiscible liquid, the lens shape is governed by this force balance, the resultant of which is zero (Fig. 2). Equation (2) can also be derived by energy minimization considerations.

The spreading of the drop can be characterized by a spreading coefficient:

$$S = \gamma_{SV} - \gamma_{SL} - \gamma_{LV}\,. \tag{3}$$

If $S \geqslant 0$, complete spreading occurs in which the drop spontaneously forms a liquid film above the solid substrate, as shown in Fig. 3(a), due to a decrease in the free energy. If $S < 0$, $\theta > 0°$ from Eq. (2) and the drop spreads to an equilibrium shape, constrained by the contact line where the three phases meet; if $\theta < 90°$, the surface is said to be *hydrophilic* (Fig. 3(b)) whereas the surface is said to be *hydrophobic* if $\theta > 90°$ (Fig. 3(c)). Strictly speaking, there is no local minimum in the interfacial energy for $S > 0$ and hence the equilibrium contact angle $\cos\theta$ cannot be defined by Eq. (2). The minimum is defined at $S = 0$, which from Eqs. (2) and (3) gives $\cos\theta = 1$ or $\theta = 0°$, corresponding to the complete wetting case.

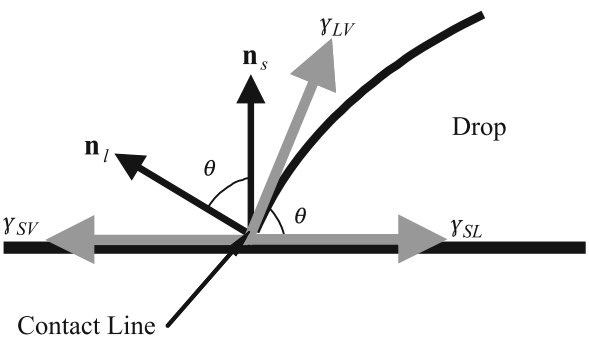

Wetting and Spreading, Figure 1 Force balance at the three-phase contact line where the solid-liquid and vapor phases meet. The outward unit normals protruding from the solid and liquid at the contact line are shown. The angle θ subtending these unit normal vectors or that subtending the interface between the drop and the solid substrate is known as the contact angle

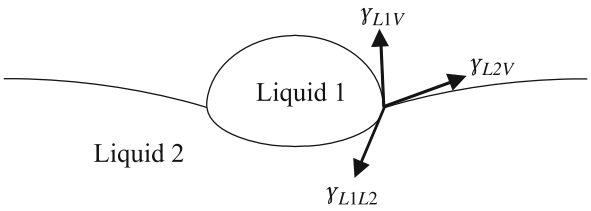

Wetting and Spreading, Figure 2 Force balance at the contact line of a liquid lens sitting above an immiscible liquid

The contact angle is known as a *static* contact angle when the contact line is stationary with respect to the solid substrate. Young's equation in Eq. (2) is therefore a description of the static contact angle. On the other hand, if the contact line is moving relative to the solid, the contact angle, whether it is advancing or receding, is known as a *dynamic* contact angle. The dynamic contact angle varies with the speed at which the contact line advances (or recedes). The upper theoretical limit of the receding contact line speed is therefore the case of complete wetting where the dynamic contact angle approaches 0°. The opposite completely non-wetting limit can be seen when the bulk of the advancing fluid and hence the drop interface overtakes the contact line and hence entrains the fluid being displaced. An example of this is in gravity driven fronts in which the advancing front of the drop forms a nose which rolls over the contact line, as shown in Fig. 4, in which case the dynamic contact angle would approach 180°; in this case, the entrained fluid is therefore the air surrounding the drop. In the extreme completely non-wetting case $\theta = 180°$, a thin submicroscopic film of the displaced phase is entrained beneath the drop therefore causing the complete disappearance of the contact line.

A point should be made here about superhydrophobic surfaces, over which a drop can translate via two states. In a suspended state, the drop sits atop the apex tips of the rough surface; air is entrained beneath the drop and fills the interstices of the rough surfaces between the apex tips. In this state, it has been shown that the velocity of the drop increases with increasing contact angles. Although this may seem contradictory to the classical view above, it is this author's view that the contact line receding speed remains low but the drop itself slides over the entrained air layer due to bulk convection. The increasing bulk drop velocity with increasing contact angles is attributed to the higher center of mass of the drop [1]. For drops in a collapsed state, wherein the liquid fills the interstices of the rough surface, the drop velocity is reduced dramatically each time the contact line reaches a cavity and a stick-slip motion is therefore observed.

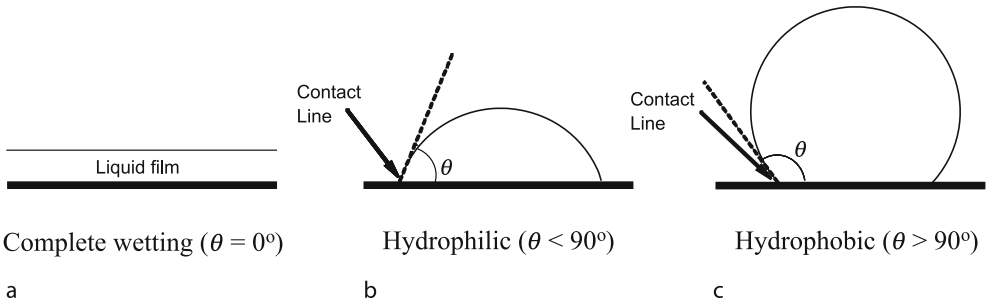

Wetting and Spreading, Figure 3 Equilibrium conditions for a liquid drop in contact with a solid substrate. (**a**) Complete wetting. (**b**) Partial wetting: hydrophilic drop. (**c**) Partial wetting: hydrophobic drop

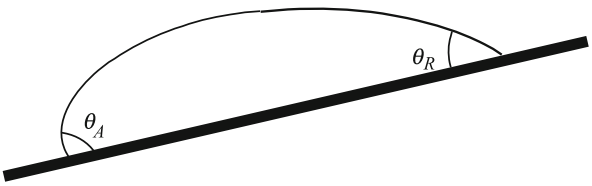

Wetting and Spreading, Figure 4 Schematic depiction of contact angle hysteresis arising when the solid substrate upon which a drop is placed is inclined. At the instance prior to the drop moving down the plane, the contact angle at the advancing front and at the rear are known as the advancing and receding contact angles, respectively

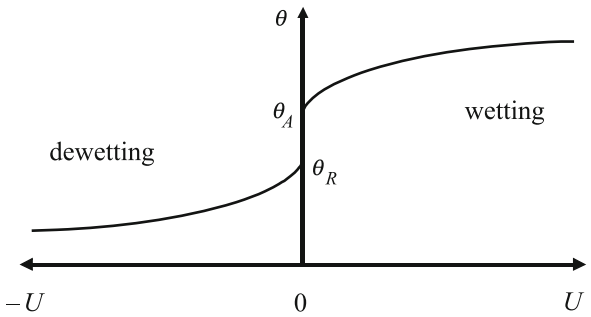

Wetting and Spreading, Figure 5 Contact angle hysteresis arising due to the dependence of the apparent contact angle θ on the contact line velocity U

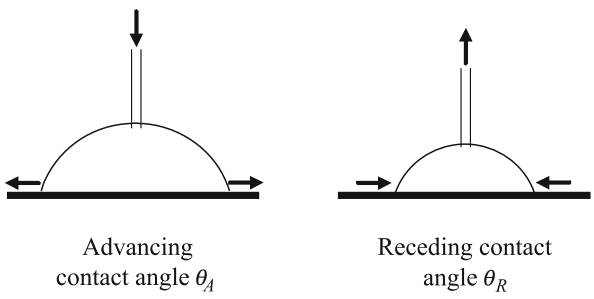

Wetting and Spreading, Figure 6 Measurement of the advancing and receding contact angles by incrementally adding or removing liquid through a thin capillary tube. The measurements are taken just prior to motion of the contact line

The boundary between the static and dynamic conditions also gives rise to contact angle hysteresis, in which the static contact angle when the contact line velocity U is zero is not single-valued (as predicted by Eq. (2)), as shown in Fig. 5, which maps out the velocity dependence of the contact angle. The static contact angle at equilibrium θ appears to be dependent on the history of the drop, i. e., on whether it is on the verge of advancing or receding. The observed contact angle at the front just before the inclined drop in Fig. 4 begins to slide is known as the *advancing* contact angle θ_{A} whereas that at the rear is known as the *receding* contact angle θ_{R}. Alternatively, the advancing and receding contact angles can be obtained by measuring the contact angle of a sessile drop just prior to motion when liquid is added or removed from a capillary above the drop to drive it to advance or recede, respectively, as illustrated in Fig. 6. The difference in the advancing and receding angles, i. e., $\theta_{\mathrm{A}} - \theta_{\mathrm{R}}$ (typically 10° or larger), is therefore the contact angle hysteresis, and the equilibrium static contact angle takes any intermediate value in between these limits, i. e., $\theta_{\mathrm{R}} \leqslant \theta \leqslant \theta_{\mathrm{A}}$.

Contact angle hysteresis can be attributed to a departure from the conditions of ideality of the solid, namely, surface roughness, chemical inhomogeneities or contamination, or, the presence of solute (polymers or surfactants) deposits on the surface [2]. Figure 7 shows a plan view illustration of the hysteresis mechanism in which the receding contact line of a drop is locally pinned when the drop moves over a localized surface inheterogeneity which is more hydrophilic than the substrate surface. As a result, there is a distortion of the contact line [3]. If the macroscopic force exerted on the contact line is

$$F = \gamma_{\mathrm{LV}} \left(\cos\theta' - \cos\theta \right) , \tag{4}$$

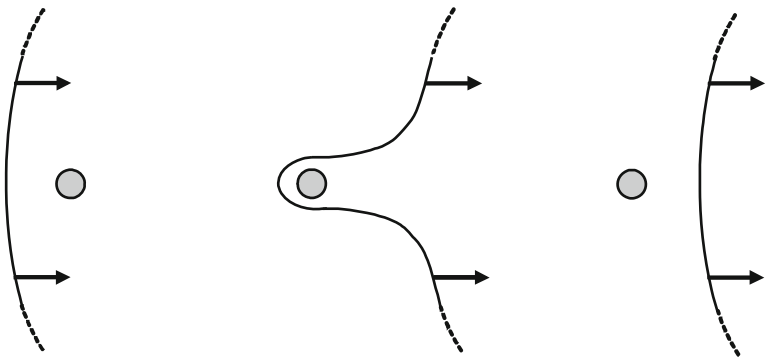

Wetting and Spreading, Figure 7 Plan view illustrating the pinning of the receding contact line due to the presence of a localized surface heterogeneity (represented by the shaded spot) which is more hydrophilic than the substrate. The arrows indicate the direction of the drop motion

where θ' is the contact angle of the drop and θ is the equilibrium contact angle given by Young's equation (Eq. (2)), we note that it is not possible to detach the contact line below a given value of the force and hence the contact line remains pinned for contact angles θ' below that of the equilibrium contact angle θ. In such cases and when evaporation is significant, there arises liquid flow from the bulk of the macroscopic drop in order to replenish the liquid evaporated from the contact line region. If solutes are present in the liquid, these are convected towards the contact line and deposited there, resulting in the formation of concentrated rings along the perimeter of the contact line; an example of this is the ubiquitous coffee-ring stain phenomenon.

A distinction between the *apparent* (or visible) contact angle θ_a and the intrinsic contact angle θ is worthy of mention. The apparent contact angle is a macroscopic extrapolation whereas the intrinsic contact angle is that microscopically subtended from the solid substrate at the contact line, as schematically depicted for a rough surface in Fig. 8. The advancing and receding contact angles due to contact angle hysteresis therefore relate to apparent contact angles. Thus, were the surface ideal, i. e., atomically smooth, clean and homogeneous such that Eq. (2) holds, then the apparent contact angle should coincide with the intrinsic contact angle to describe the equilibrium static contact angle.

Nevertheless, for most practical surfaces, this is not true and hence the intrinsic contact angle is difficult to determine. The surface heterogeneities could very well be the reason why the wetting line moves in a hesitant jerk or shuffling motion, termed as *stick-slip* motion [4]. This could also be attributed to the successive formation and collapse (due to negative disjoining pressure) of the entrained air film beneath the drop. Changes to the apparent contact angle, nevertheless, can be evaluated for rough

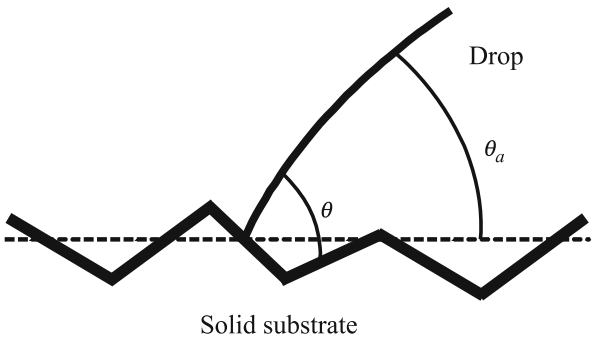

Wetting and Spreading, Figure 8 Schematic depiction of the contact line region on a microscopic level illustrating the distinction between the apparent (macroscopic) contact angle θ_a and the intrinsic (microscopic) contact angle θ due to surface roughness effects on the substrate

surfaces. Consider a small displacement of the contact line dx on a rough but chemically homogeneous surface, as shown in Fig. 9(a). The change in the surface energy per unit length along the contact line dE is then

$$dE = (\gamma_{SL} - \gamma_{SV})\, r dx + \gamma_{LV} \cos\theta^* dx\,, \tag{5}$$

in which r is the surface roughness (assumed to be much smaller than the macroscopic drop length scale) and θ^* denotes the contact angle on the rough surface ($r > 1$).

At equilibrium, the resultant surface forces at the contact line balance and hence the energy is at its minimum, i. e., $dE/dx = 0$. Wenzel's law, derived from this equilibrium condition $dE/dx = 0$ together with Eq. (2) (which can be recovered from Eq. (5) for smooth surfaces where, by definition, $r = 1$), then states

$$\cos\theta^* = r\cos\theta\,, \tag{6}$$

wherein θ is the contact angle for smooth surfaces given by Young's equation (Eq. (2)). Since $r > 1$ for rough surfaces, $|\cos\theta^*| > |\cos\theta|$, implying that surface heterogeneities always act to amplify the inherent properties of a surface. In other words, a hydrophilic surface ($\theta < 90°$) will be rendered more hydrophilic ($\theta^* < \theta$) and a hydrophobic surface ($\theta > 90°$) will be rendered more hydrophobic ($\theta^* > \theta$) in the presence of surface roughness.

A similar analysis can be carried out for physically smooth but chemically inhomogeneous surfaces, as depicted in Fig. 9(b), where we allow the surface to comprise of two different materials, each of which is associated with a corresponding contact angle, θ_1 and θ_2. Denoting the fractions along the surface which is composed by each material as f_1 and f_2 (such that $f_1 + f_2 = 1$), assuming f_1 and f_2 are small compared to the area occupied by the entire drop, Eq. (5) now becomes

$$\mathrm{d}E = f_1\,(\gamma_{\mathrm{SL}} - \gamma_{\mathrm{SV}})_1\,\mathrm{d}x + f_2\,(\gamma_{\mathrm{SL}} - \gamma_{\mathrm{SV}})\,2\mathrm{d}x + \gamma_{\mathrm{LV}}\cos\theta^*\mathrm{d}x\,. \tag{7}$$

Energy minimization then requires

$$\cos\theta^* = f_1\cos\theta_1 + f_2\cos\theta_2\,, \tag{8}$$

which is known as the Cassie–Baxter law. In this case, the apparent contact angle due to the chemical inhomogeneous surface is the average of the cosines of the contact angles associated with each chemical that the surface is comprised of, and is hence bounded by the two extremes of these contact angles.

Capillarity

The equilibrium drop shape is related to the surface tension of the drop through its curvature. In other words, the tendency for the drop to assume a curved interfacial shape is due to its surface tension. A consequence of this is the existence of a pressure difference across the interface

$$\Delta p = \gamma_{\mathrm{LV}}\kappa\,, \tag{9}$$

with the highest pressure residing on the concave side.

$$\kappa = \frac{1}{R_1} + \frac{1}{R_2}\,, \tag{10}$$

is twice the mean curvature wherein R_1 and R_2 are known as the principal radii of curvature, which is the radii of curvature of the interface along any two orthogonal elements. Equation (9) is known as the *Laplace–Young equation*. For a spherical drop or bubble, $R_1 = R_2 = R$ and hence

$$\Delta p = p_{\mathrm{i}} - p_{\mathrm{e}} = \frac{2\gamma_{\mathrm{LV}}}{R}\,, \tag{11}$$

where p_{i} and p_{e} are the pressures inside and outside the drop or bubble, respectively.

Capillarity is the phenomena that arises due to the existence of a finite (or even zero) contact angle that a liquid makes with the solid substrate. One example is the height-of-rise of a liquid in an open capillary tube, as shown in Fig. 10. The associated liquid motion due to surface tension is known as *capillary flow*. Assuming the meniscus to be approximately hemispherical with constant radius of curvature $R_1 = R_2 = R/\cos\theta$, where $2R$ is the capillary diameter, the pressure variation across the interface from Eq. (11) is then

$$\Delta p = p_{\mathrm{atm}} - p_{\mathrm{liq}} = \frac{2\gamma_{\mathrm{LV}}\cos\theta}{R}\,, \tag{12}$$

where p_{atm} and p_{liq} are the atmospheric and liquid pressures, respectively. Given that at equilibrium, the hydrostatic head of the liquid capillary $p_{\mathrm{liq}} + \rho g H$, where ρ is the liquid density, g the gravitational acceleration and H the equilibrium height of the liquid capillary column, must balance the atmospheric pressure, i. e.,

$$p_{\mathrm{liq}} + \rho g H = p_{\mathrm{atm}}\,, \tag{13}$$

H can then be obtained by substituting Eq. (12):

$$H = \frac{2\gamma_{\mathrm{LV}}\cos\theta}{\rho g R}\,. \tag{14}$$

Equation (14) therefore represents an equilibrium dominant balance between the gravitational and surface tension forces. Thus, given that ρ and $\cos\theta$ are known for a given fluid, the capillary rise can be determined. It is also evident from Eq. (14) that the capillary rise is dependent on the capillary radius. For small capillaries, H can therefore become relatively large. This capillary rise method is therefore very useful and accurate for measuring the surface tension of liquids.

Key Research Findings

Spreading Dynamics

We briefly consider the spreading dynamics of a drop, sufficiently small such that the spreading is not influenced by gravity. We will also assume the substrate to be smooth and homogeneous since surface roughness effects can enhance spreading and even lead to the spontaneous wetting of partially wetting liquids. The interface is also assumed to be

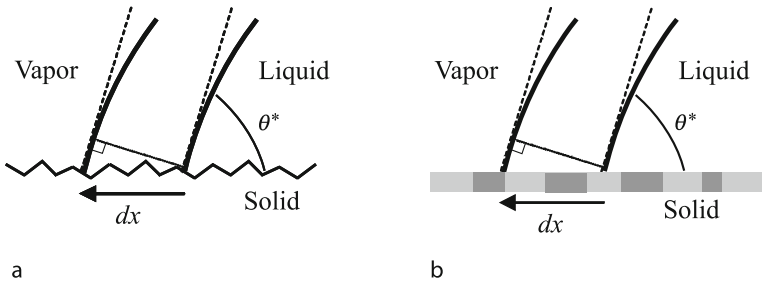

Wetting and Spreading, Figure 9 Contact line region of a drop on a (**a**) physically rough but chemically homogeneous surface, and, (**b**) a physically smooth but chemically inhomogeneous surface consisting of two different surface materials. A small displacement to the contact line dx is considered in the derivation of Wenzel's law in the case of (**a**) and the Cassie–Baxter law in the case of (**b**)

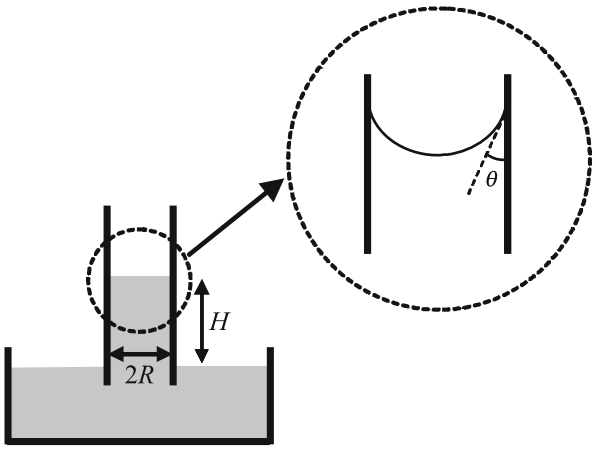

Wetting and Spreading, Figure 10 Schematic depiction of a capillary height-of-rise experiment

clean such that no surface tension gradients are imposed, which could lead to Marangoni stresses; such effects will be discussed subsequently. The experimentally observed spreading data for complete wetting then appears to follow a simple power law relationship given by

$$R(t) \sim t^n , \tag{15}$$

where R is the radius of the spreading drop and t denotes time. n has been empirically found to lie between 0.1 and 0.14; it's value has been reported to be dependent on the drop volume, temperature and physical properties as well as the humidity of the ambient phase.

There is also a very specific scaling for the macroscopic dynamic contact angle θ. This was first observed by Hoffman [5], who investigated the variation in the contact angle of an advancing meniscus front in a capillary tube subject to different fluid driving velocities, as well as Tanner [6], who observed similar behavior for drops spreading on a horizontal substrate. In both cases, it was observed that for small Ca,

$$\theta \sim \mathrm{Ca}^{\frac{1}{3}} , \tag{16}$$

where

$$\mathrm{Ca} \equiv \frac{\mu U}{\gamma} , \tag{17}$$

is the capillary number with $U(t) = \mathrm{d}R(t)/\mathrm{d}t$ being the speed of the contact line in the above, μ is the viscosity. The universal law given by Eq. (16) has since been corroborated by many investigators.

Kalliadasis and Chang [7] considered the behavior of the asymptotic region between the bulk macroscopic drop and a thin film ahead of the drop in which liquid from the perfectly wetting drop drains into due to the negative disjoining and capillary pressures, as shown in Fig. 11. This thin film, known as the precursor film, has both been observed experimentally [8] and is also used as a convenient means of removing mathematical difficulties near the contact line region where continuum theory breaks down; a discussion of this will be carried out below. In this asymptotic region between the bulk drop, of characteristic length scale L, and the precursor film region, of characteristic length scale $\hat{L}$, viscous and capillary forces dominate.

Thus, assuming the film in this region to be thin such that the lubrication approximation holds, the spreading dynamics of the drop in the limit $\hat{L}/L \ll 1$ and the local quasi-steady limit with respect to a moving coordinate frame translating at a constant dimensionless speed given by Ca, is governed by the Bretherton [9] equation:

$$3\,\mathrm{Ca}\frac{\partial h}{\partial x} = \frac{\partial}{\partial x}\left(h^3 \frac{\partial^3 h}{\partial x^3}\right) , \tag{18}$$

where h is the dimensionless film height, scaled by the characteristic height of the macroscopic drop H. In the

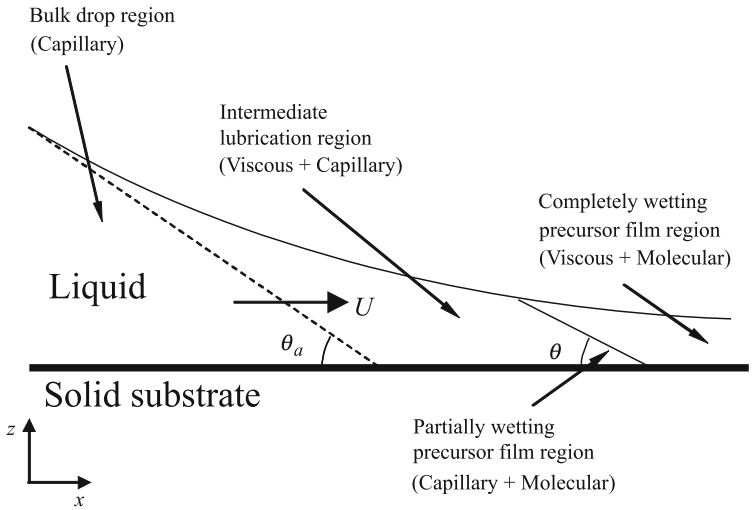

Wetting and Spreading, Figure 11 Contact line region of a spreading drop ahead of which a thin front running precursor film exists. The intermediate asymptotic region where viscous and capillary forces dominate is shown. After Kalliadasis and Chang [7]

above, the axial and vertical coordinates, x and z are scaled by L and H, respectively. Kalliadasis and Chang [7] then showed that the film height, upon redimensionalization, assumes the following weak logarithmic behavior as it asymptotes away from the contact line:

$$h \sim -x\,\mathrm{Ca}^{\frac{1}{3}} \left(9 \log \frac{\hat{L}}{L}\right)^{\frac{1}{3}} . \tag{19}$$

A dynamic contact angle condition can then be written for the macroscopic spreading drop:

$$\tan\theta \sim -\frac{\partial h}{\partial x} \sim \left(-9 \log \frac{\hat{L}}{L}\right)^{\frac{1}{3}} \mathrm{Ca}^{\frac{1}{3}} , \tag{20}$$

showing that the local quasi-steady spreading of a partially or completely wetting liquid drop at constant speed Ca driven by viscous and capillary forces always gives rise to an interfacial shape that scales consistently with the universal law given in Eq. (16). Equation (20) suggests that away from the static equilibrium limit, a partially wetting drop behaves, albeit quite surprisingly, like a complete wetting drop, consistent with the experimental findings for sufficiently large Ca [7].

It is now possible to insert this dynamic contact angle condition back into the spreading relationship in Eq. (15) to obtain an explicit power law for the spreading dynamics of a drop lying on a horizontal substrate [7]. If the drop can be assumed to be thin, then the axisymmetric Laplace–Young equation in the lubrication limit reads

$$\frac{\partial}{\partial r}\left[\frac{1}{r}\frac{\partial}{\partial r}\left(r\frac{\partial h}{\partial r}\right)\right] = 0 . \tag{21}$$

The following boundary conditions apply

$$\frac{\partial h}{\partial r}(r=0) = 0 , \quad h(r=R) = 0 , \quad \text{and,}$$
$$\frac{\partial h}{\partial r}(r=R) = -\tan\theta . \tag{22}$$

In addition, we impose conservation of the drop volume V:

$$\int_0^R hr\,\mathrm{d}r = \frac{V}{2\pi} . \tag{23}$$

Integrating Eq. (21) twice subject to the boundary conditions above then yields

$$h(r) = \frac{2V}{\pi R^2}\left[1 - \left(\frac{r}{R}\right)^2\right] . \tag{24}$$

Substitution of the dynamic contact angle condition in Eq. (20) then gives

$$\frac{\partial h}{\partial r}(r=R) = -\frac{4V}{\pi R^3} = \left(9 \log \frac{\hat{L}}{L}\right)^{\frac{1}{3}} \mathrm{Ca}^{\frac{1}{3}} . \tag{25}$$

Since the dimensionless advancing speed of the contact line can be written as $\mathrm{d}R/\mathrm{d}t = 3\,\mathrm{Ca}$, where time is scaled

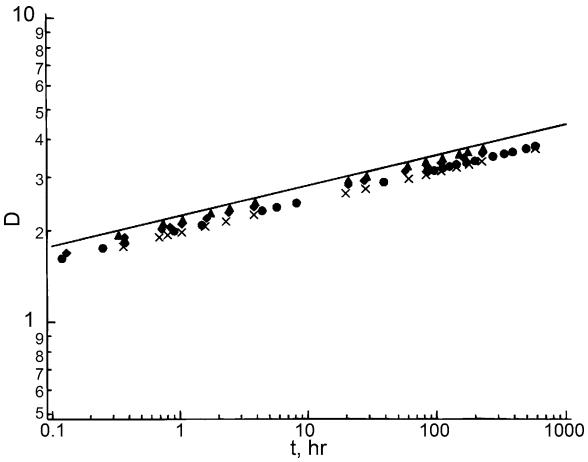

Wetting and Spreading, Figure 12 Collapse of the poly(dimethylsiloxane) drop spreading data of Ausserré et al. [8] with the dimensional form of the universal law given by integration of Eq. (26), which is denoted by *D*. Reproduced with permission from [8]

by $\mu L/\gamma$ and the radius by $V^{1/3}$, it then follows that

$$\frac{\partial R}{\partial t} = -\frac{512V}{3\log\left(\hat{L}/L\right)R^9}, \tag{26}$$

and hence

$$R \sim t^{\frac{1}{10}}, \tag{27}$$

consistent with the dynamic spreading law of Eq. (15). The collapse of the experimental data of [8] for the spreading of poly(dimethylsiloxane) drops of various volumes on a silicon substrate is shown in Fig. 12 [7]. On the other hand, for large drops where gravity would play an influence, the drop radius would spread as $R \sim t^{1/8}$ instead.

Stress Singularity

In addition to the challenges in the treatment of free surfaces, dynamic spreading models encounter a significant conceptual difficulty due to the breakdown of continuum hydrodynamics at the contact line when the sharp continuum interface is extrapolated to molecular scales to define the contact angle. At these microscopic scales, such geometric conceptualizations such as an interface and the contact angle becomes ambiguous. Moreover, the enforcement of the slip-free and tangential stress continuity on the smooth solid substrate at the three-phase contact line gives rise to a stress singularity [4]. In other words, a logarithmically infinite force is required to advance the contact line, which is not observed experimentally [10]. This locally unbounded force is not the result of a kinematic incompatibility between the no-slip condition on the substrate and the existence of an advancing drop interface that is impenetrable by both sides of the fluid [11]. Instead, Dussan and Davis [11] suggest that the stress singularity is a dynamic consequence of the multi-valued velocity field at the contact line.

Various models have been proposed to overcome this difficulty. Early models allowed the continuum theory to define the contact angle up to a molecular cut-off. One approach is to allow for a finite slip velocity such that the stress singularity, whilst not removed altogether, becomes a logarithmic singularity that is at least integrable [12, 13]. Another approach that we have discussed above is to assume that a thin precursor film precoats the substrate [14]. Alternatively, given that wetting is driven by molecular forces at the inner region of the contact line, the disjoining pressure arising from long-range intermolecular interactions can be introduced to account for a negative pressure that sucks liquid from the bulk into the precursor film.

Nevertheless, it has been shown that the same asymptotic behavior of the inner region away from the contact line given by the universal solution of Eq. (19) is recovered regardless of which model above is adopted to remove the contact line stress singularity in both partially or completely wetting fluids [15]. In fact, the dimensionless length scale $\hat{L}/L$ can be shown to be equal to the precursor film thickness b, i. e.,

$$\frac{\hat{L}}{L} \sim \frac{b}{H}, \tag{28}$$

if the precursor film is adopted, the Hamaker constant α, i. e.,

$$\frac{\hat{L}}{L} \sim \frac{1}{L}\left(\frac{|\alpha|}{6\pi\gamma}\right)^{\frac{1}{2}}, \tag{29}$$

if the disjoining pressure is used, and, the slip coefficient $\lambda_i = \lambda h^i$, i. e.,

$$\frac{\hat{L}}{L} \sim \lambda_i^{\frac{1}{(1+i)}}, \tag{30}$$

if a slip model is employed; λ is the film thickness dependent slip length, the dependence of which is given by the exponent i $(=0, 1)$ and corresponds to the different slip models historically used [16].

To leading order, the intermolecular forces are shown to be solely determined by the apparent dynamic contact angle and independent of slip. The precursor film is also shown to be reasonable approximation to account for intermolecular effects although both the precursor film and slip

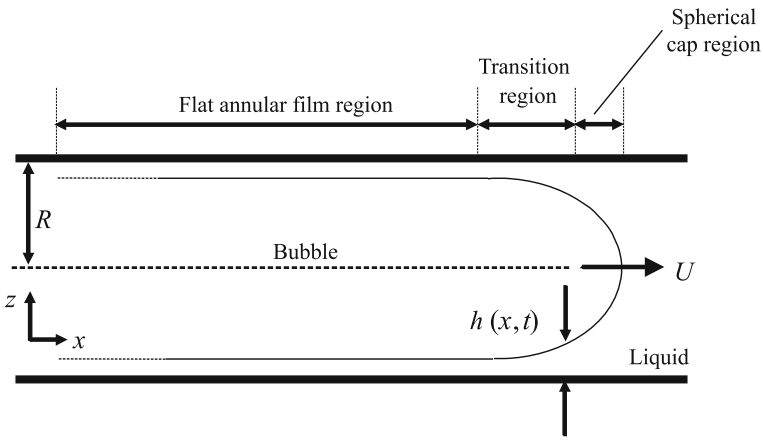

Wetting and Spreading, Figure 13 Schematic depiction of a bubble translating within a long capillary tube

models, while mathematically convenient for handling the problem of stress singularity, do not appear to contribute to the dynamic contact angle condition. In any case, imposing one or the other does not lead to significant error due to the weak dependence of the coefficient $-9\log(\hat{L}/L)$ on the asymptotic behavior of the bulk drop region [15].

Capillary Driven Spreading

We have already observed an example of capillary-driven spreading in the capillary rise experiment described above. Another example of capillarity is that of bubble transport in capillary tubes [9]. Scaling arguments for this problem, illustrated in Fig. 13, are discussed by Chang [17]. To leading order, the pressure drop at the front and rear spherical caps are given by Eq. (11) and thus the axial curvature is $1/R$, where R is the radius of curvature of the bubble cap. In the short intermediate transition region of length L_0 between the spherical cap and annular film regions, the azimuthal curvature gradient, which scales as H_0/R^2L_0 given that the azimuthal curvature is $1/(R-h)$, is negligible compared to the axial curvature gradient, which scales as H_0/L_0^3 since the axial curvature is $\mathrm{d}^2h/\mathrm{d}x^2$ (that $L_0 \ll R$ will be explicitly shown below in Eq. (33)); h is the liquid film thickness with a characteristic length scale in the transition region of H_0 and x is the axial coordinate. Asymptotic matching between the transition and cap regions then gives rise to a balance between the axial and azimuthal curvatures:

$$\frac{H_0}{L_0^2} \sim \frac{1}{R}\,. \tag{31}$$

A balance between viscous and capillary forces requires

$$\frac{\mu U}{H_0^2} \sim \frac{\mathrm{d}p}{\mathrm{d}x} \sim \frac{\gamma}{RL_0}\,, \tag{32}$$

where U is the speed of the bubble. It then follows from Eqs. (31) and (32), with the dimensionless speed Ca defined by Eq. (17), that

$$H_0 \sim R\,\mathrm{Ca}^{\frac{2}{3}}\,, \text{ and }, \quad L_0 \sim R\,\mathrm{Ca}^{\frac{1}{3}}\,, \tag{33}$$

as long as $\mathrm{Ca} \ll 1$.

To render the problem quasi-steady, a moving coordinate frame is adopted such that the bubble translates at speed Ca. In the thin annular film region, application of the lubrication approximation to a balance between viscous and capillary forces then yields the following dimensionless equation for the film thickness h [17]:

$$h^3\frac{\mathrm{d}^3h}{\mathrm{d}x^3} = h - 1\,, \tag{34}$$

where h is scaled by the characteristic height of the film H_0 and x by $H_0(3\,\mathrm{Ca})^{-1/3}$. Equation (29) describes the asymptotic behavior in the transition regions for both the front spherical cap as $x \to \infty$ and the rear spherical cap as $x \to -\infty$. Since a quadratically increasing film height is expected, we allow

$$h = A^{\pm}x^2 + B^{\pm}x + C^{\pm}\,, \tag{35}$$

where A, B and C are constants in which the $+$ subscript denotes that pertaining to the front cap and the $-$ subscript pertains to the rear cap. These can be obtained by numerical integration of Eq. (34) starting from the flat film where $\mathrm{d}h/\mathrm{d}x = \mathrm{d}^2h/\mathrm{d}x^2 = 0$, noting that B can be set to zero by arbitrarily shifting the origin. It is then possible to match the curvature $\mathrm{d}^2h/\mathrm{d}x^2$ of the asymptotic solution in Eq. (35) to the outer spherical cap solutions, which to

leading order, are static solutions of the Laplace–Young equation. Chang [17] showed that this leads to

$$\frac{H_0}{R} = 0.643\,(3\,\mathrm{Ca})^{\frac{2}{3}}\ , \tag{36}$$

which is an estimate of the film thickness to leading order. Similar scalings can also be observed in coating flows wherein solid substrates are coated with a thin and uniform liquid film.

Marangoni and Thermocapillary Driven Spreading

In our discussion above, we had assumed that the interface is clean and isothermal. However, surface impurities and non-uniform temperatures can alter the local surface tension, thus giving rise to surface tension gradients that generate additional interfacial stresses, the so-called Marangoni stresses [18]. Marangoni stresses can, in turn, alter the macroscopic spreading behavior significantly and introduce instabilities at the spreading front. Troian et al. [14] have shown that a capillary ridge appears at the advancing front which is the target of viscous instabilities that lead to a fingering phenomenon. Away from the spreading front, instabilities arising from surfactant concentration or thermal non-uniformities can also give rise to dewetting and hence the formation of dry-spots upon rupture of the liquid film [19, 20].

Future Directions for Research

Despite considerable advances in the investigations carried out on wetting and spreading phenomena over several decades, a complete fundamental understanding is still elusive, particularly at the contact line where significant conceptual and mathematical difficulties arise. Although it has been seen above that the weak logarithmic asymptotic behavior in the contact line region suggests that an intimate knowledge of the microscopic conditions is not required to accurately model the macroscopic spreading behavior, the local microscopic wetting behavior may still be important in many physical systems, and particularly so where nanochannel wetting and transport at molecular scales, are concerned. As such, there is a further need to verify and successively refine our current understanding concerning microscopic wetting dynamics.

This is now possible due to advances in computer processing, which has previously limited the scope of molecular dynamics (MD) simulations in microscopically modeling local dynamic wetting behavior. By integrating the laws of motion governing individual molecular particles and taking into account intermolecular interactions, it is possible to resolve the velocity fields which then provide a mechanism for slippage of liquid molecules over the solid. In addition, dynamic contact angle conditions can be inferred and appear to be dependent on the interaction potentials between the liquid and solid molecules. Nevertheless, MD simulations are still confined to small length scales and continue to be limited to short times. As such, it is envisaged that multi-scale spatial and time averaging techniques will allow a unified coupling between continuum and molecular theories to provide a more complete description for modeling wetting behavior. A description of such multiscale models is given in Karniadakis et al. [21]. MD simulations involving equilibrium statistical mechanics or weak deviations from equilibrium (for example, by means of density-functional theories), can therefore replace the disjoining pressure in molecular theories to explicitly account for intermolecular interactions in an intermediary step in asymptotic matching with continuum hydrodynamic models in the long scale limit.

Cross References

- ► Applications Based on Electrowetting
- ► Bubble Dynamics in Microchannel
- ► Capillary Filling
- ► Digital Microfluidics
- ► Droplet and Bubble Formation in Microchannels
- ► Droplet Based Lab-on-a-Chip Devices
- ► Droplet Dispensing
- ► Droplet Dynamics in Microchannel
- ► Electrocapillary
- ► Electrowetting
- ► Electrowetting and Droplets
- ► Interfacial Electrokinetic Flow
- ► Surface Tension Driven Flow
- ► Surface Tension, Capillarity and Contact Angle
- ► Thermal Capillary
- ► Thermocapillary Pumping

References

1. Dupuis A, Yeomans JM (2006) Dynamics of sliding drops on superhydrophobic surfaces. Europhys Lett 75:105–111
2. de Gennes PG (1985) Wetting: statics and dynamics. Rev Modern Phys 57:827–863
3. Nadkarni GD, Garoff S (1992) An investigation of microscopic aspects of contact angle hysteresis: Pinning of the contact line on a single defect. Europhys Lett 20:523–528
4. Huh C, Scriven LE (1971) Hydrodynamic model of steady movement of a solid/liquid/fluid contact line. J Colloid Interface Sci 35:85–101
5. Hoffman RL (1975) A study of the advancing interface. I. Interface shape in liquid–gas systems. J Colloid Interface Sci 50:228–241

6. Tanner LH (1979) The spreading of silicone oil drops on horizontal surfaces. J Phys D: Appl Phys 12:1473–1484
7. Kalliadasis S, Chang H-C (1996) Dynamics of liquid spreading on solid surfaces. Ind Eng Chemistry Res 35:2860–2874
8. Ausserré D, Picard AM, Léger L (1986) Existence and role of the precursor film in the spreading of polymer liquids. Phys Rev Lett 57:2671–2674
9. Bretherton FP (1961) The motion of long bubbles in tubes. J Fluid Mech 10:166–188
10. Kistler SF (1993) Hydrodynamics of wetting. In: Berg JC (ed) Wettability. Marcel-Dekker, New York
11. Dussan V EB, Davis SH (1974) On the motion of a fluid-fluid interface along a solid surface. J Fluid Mech 65:71–96
12. Hocking LM (1977) A moving fluid interface. Part 2. The removal of the force singularity by a slip flow. J Fluid Mech 79:209–229
13. Dussan V EB (1979) On the spreading of liquids on solid surfaces: Static and dynamic contact lines. Ann Rev Fluid Mech 11:371–400
14. Troian SM, Herbolzheimer E, Safran SA, Joanny JF (1989) Fingering instabilities of driven spreading films. Europhys Lett 10:25–30
15. Yeo LY, Chang H-C (2006) Electrowetting films on parallel line electrodes. Phys Rev E 73:011605
16. Haley PJ, Miksis MJ (1991) The effect of the contact line on droplet spreading. J Fluid Mech 223:57–81
17. Chang H-C (2002) Bubble/Drop transport in microchannels. In: Gad-el Hak M (ed) The MEMS Handbook. CRC Press, Boca Raton
18. Edwards DA, Brenner H, Wasan DT (1991) Interfacial transport processes and rheology. Butterworth-Heinemann, London
19. Warner MRE, Craster RV, Matar OK (2002) Dewetting of ultra-thin surfactant-covered films. Phys Fluids 14:4040–4054
20. Yeo LY, Craster RV, Matar OK (2003) Marangoni instability of a thin liquid film resting on a locally heated horizontal wall. Phys Rev E 67:056315
21. Karniadakis G, Beskok A, Aluru N (2005) Microflows and Nanoflows. Springer, New York

Wetting on Structured Substrates

► Surface-Directed Capillary Flow Systems

Wien Filter

► Crossed Field Filter

World-to-Chip Interface

► Transferring Samples to Chips, Techniques